SOFT ROBOTICS
Volume 00, Number 00, 2018

DOI: 10.1089/soro.2018.0053

SoRo
Soft Robotics

Agile and Resilient Insect-Scale Robot

Tiefeng Li,[1–5] Zhanan Zou,[1,2] Guoyong Mao,[1–3] Xuxu Yang,[1–3] Yiming Liang,[1–3] Chi Li,[1,2] Shaoxing Qu,[1–5] Zhigang Suo,[6] and Wei Yang[1,3,5]

Abstract

A key challenge in bioinspired insect-scale running robots is to make them both agile and resilient. In this study, we develop a dielectric elastomer actuated soft robot that mimics inchworms. We use an elastomer to make the soft body, a stretchable dielectric to provide electrostatic actuation of high power density, and multizone actuation to achieve ratcheting locomotion. We fabricate the body, muscles, and feet in a single piece, with no internal open space. The robot runs four times its body length per second and turns at a radius about three times its body length in 0.3 s. The robot survives compression 30,000 times its own weight and survives collision with a rigid surface at a speed of 30 m/s. The robot can climb a slope of 30°. Walking on a horizontal plane, the robot carries a payload four times its own weight. The robot can operate on land, underwater, and in vacuum. The simplicity in design and fabrication will enable the robot to serve as a model system to investigate insect-scale actuation and locomotion, as well as the social behavior of swarms of robots. The robot also provides a platform to integrate wireless charging, mobile communication, and stretchable electronics.

Keywords: soft robot, dielectric elastomer, bioinspired, ratcheting locomotion

Introduction

Inchworms, beetles, and cockroaches are agile and resilient.[1] They run, turn, and stop quickly. They survive compression many times their own weights and survive falling from arbitrary height. Their agility and resilience derive from soft bodies and powerful muscles. They have inspired the development of insect-scale robots for reconnaissance or delivering payloads to locations difficult to access.[2,3] Existing insect-scale running robots, however, are slow or fragile. Biologically inspired robots with soft or partially soft bodies have the potential to be more robust and adaptable, as well as safer for human interaction than traditional rigid robots.[4–14] Key challenges in the design and manufacture of soft robots include the complex fabrication processes and the interfacing of soft and rigid components. Recent advances have demonstrated insect-scale robots that crawl, run, fly, and swim.[15] They provide interactive entertainment, go on reconnaissance missions, and deliver payloads to locations difficult to access. It has been particularly challenging to make insect-scale robots both agile and resilient. A small robot should not aim to resist natural environment but adapt to it. The development of the soft-bodied robots requires new methods of sensing and actuation using soft materials.

Enormous progress has been made in the development of new methods of sensing using soft materials, as highlighted in related fields of bio-integrated and wearable electronics.[16–21] By contrast, the development of actuation has lagged behind. Existing soft robots use actuation mechanisms such as shape memory materials, responsive hydrogels, ionic polymer metal composites, pneumatics, and hydraulics.[3,22] These actuation mechanisms are either low or limited by the external environment of various hydraulic pressures and temperatures. Dielectric elastomers (DEs) have emerged as promising actuators, owing to their lightweight, giant deformation, fast response, and low cost.[23–25] Subjected to an electric field through its thickness, a DE membrane reduces

[1]Department of Engineering Mechanics, Zhejiang University, Hangzhou, China.
[2]Soft Matter Research Centre (SMRC), Zhejiang University, Hangzhou, China.
[3]Key Laboratory of Soft Machines and Smart Devices of Zhejiang Province, Hangzhou, China.
[4]State Key Laboratory of Fluid Power and Mechatronic System, Zhejiang University, Hangzhou, China.
[5]Center for X-Mechanics, Zhejiang University, Hangzhou, China.
[6]John A. Paulson School of Engineering and Applied Sciences, Kavli Institute for Nanobio Science and Technology, Harvard University, Cambridge, Massachusetts.

thickness and expands area. However, existing DE actuators[26,27] require rigid frames and high input voltage, which hinders the application of DE in soft robots.[9] To date, no agile and resilient robots using DE have been demonstrated.

In this study, we describe an agile and resilient robot using DEs. Our robot mimics inchworms. During running and turning, an inchworm bends and expands its body, switching the friction of its front and hind prolegs. This mechanism of locomotion has been simplified in the robot. The robot has a hybrid structure: a prestretched DE membrane serves as soft muscle and an elastomeric frame serves as soft body. The DE membranes and the elastomeric frame are laminated in a single piece with no internal open space. The elastomeric frame interacts with the DE membranes, providing large deformation and surviving external mechanical abuse. The patterned electrodes are coated on the multilayered DE membranes, which form various independently activated regions. Fast moving and controllable turning can be realized by applying voltages on those regions. The robot is agile when operated near the resonance. During the operation, the soft robot generates relatively low noise.

Materials and Methods

Materials

The body of the soft robot is made by the mixture of silicone and silicon dioxide particles. Silicon dioxide nanoparticles (diameter of 100 nm) are dispersed into silicone solution (Ecoflex 00–30) and blended for 40 min. The mass fraction of silicon dioxide is 5%. The elastomeric composite is cured in oven at 29°C for 5 h. The DE membranes (VHB 4910 [3M] and VHB 9473 [3M]) are cut into the designed shape by using a laser cutter (VersaLaser VLS3.50; Universal Laser Systems). The tin foils (thickness of 0.08 mm) are cut into strips with the width of 3 mm as feed lines. DE actuators are fabricated using the MG Chemicals Carbon Conductive Grease 846-80G as the compliant electrodes.

Fabrication

We fabricate the robot by integrating components of muscles, body, and feet. The muscles of the robot consist of four prestretched membranes A, B, C, and D of a DE (Fig. 1A). Membranes A and D serve as protecting layers. Membrane B is coated with a ground electrode on its top face. Membrane C is coated with another ground electrode on the bottom face, and two separate electrodes and feed lines on the top face. These electrodes are deformable and define two regions in the DE membranes as the left and right muscles. The membranes are laminated and placed between a base and a mold (Fig. 1B). The body of the robot is made of another stiffer elastomer filled into the empty space of the mold and cured (Fig. 1C). After removing the mold, the prestretched DE membranes contract and bend the body, forming the robot in the rest state (Fig. 1D). A front foot and two hind feet are three stiff hooks punctured into the body (Fig. 1E). The three hooks point to the backward direction of the robot and will act as ratchets. The left and the right muscles have separated feed lines and are independently actuated (Fig. 1F). The details of the fabrication are described as follows.

To achieve a compact and effective structure for running forward and turning, we chose a triangle-shaped structure as the soft body, right and left DE actuator as the muscles, and three feet (one front foot and two hind feet) of the robot. This design enables the robot to drive forward at full speed with the actuation of both the right and left muscles. The robot can twist its body when the voltage is only applied on one of the left or right muscle, turning the robot to the right or left correspondingly (described in the Actuation of the Soft Robot section, Fig. 3C). While VHB 4910 has been marketed as adhesive tapes, this adhesion property plays a significant role in the fabrication of the device. The VHB 4910 membranes were prestretched (2×2 biaxially prestretched) to enhance the performance. Silicone–silicon dioxide composites are cast on the membrane laminates as the elastomeric body of the robot. The acrylonitrile-butadiene-styrene plastic plates (thickness of

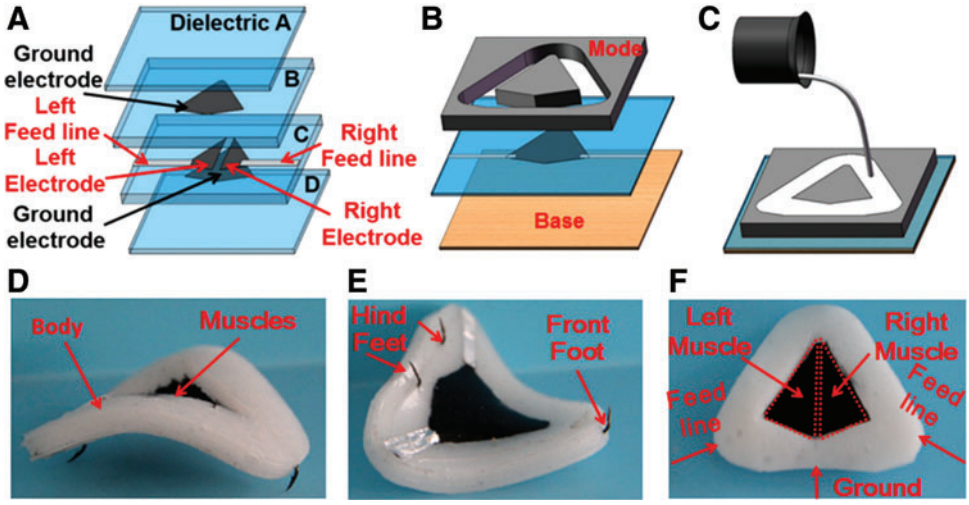

FIG. 1. Fabrication. **(A)** Four DE membranes are prestretched and laminated to form the muscles of the robot. DE membranes A and D are protecting layers. DE membrane B has a ground electrode on the top. DE membrane C has two input electrodes on the top and a ground electrode on the bottom. The electrodes are compliant, but the feed lines need not be. **(B)** The prestretched laminate is placed between a mold and a base. **(C)** Pour and cure silicone to form the body of the robot. **(D)** Upon demolding, the robot bends to its rest state. **(E)** Three stiff hooks serve as feet. **(F)** Left and right muscles can activate separately. Color images available online at www.liebertpub.com/soro

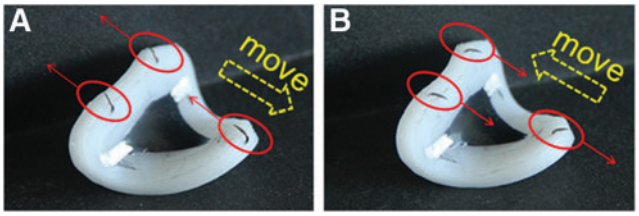

FIG. 2. Stiff hooks as the biased ratchets. **(A)** Metallic hooks tilted to the bottom of the triangle-like robot body, the robot will locomote toward the head. **(B)** Metallic hooks tilted to the head of the triangle-like robot body, the robot will locomote toward the bottom end. Color images available online at www.liebertpub.com/soro

2 mm) are laser cutted to form the mold and put on the top of the membrane laminates. Silicone–silicon dioxide composites are cast into the mold. The elastomeric composite is cured in oven at 29°C for 5 h. Silicone–silicon dioxide composites strongly adhere on the top of the VHB laminates. When demolded, the elastomeric body is bended by the prestretched laminates. Three metallic hooks (red circles in Fig. 2) are punctured into the elastomeric body to serve as biased ratchets. The tilting direction of the metallic hooks can be tuned during fabricating the robot, offering different bias during locomotion.

Actuation of the soft robot

The soft robot is powered by wired voltage source, a signal generator (Agilent 33220A) and a voltage amplifier (TREK-610E) combined to generate the high voltage. The high voltages are applied to the left and right muscles of the soft robot during the running and turning. We actuate the robot by applying voltages through the two feed lines using a power source and an external circuit. When voltages in both feed lines V_L and V_R are turned off, the robot is in a rest state (Fig. 3A). When a voltage is applied to the left muscle, for example, electric charges accumulate on the electrodes, and the electrostatic forces cause the left muscle to deform (Fig. 3B). To further investigate the voltage-induced actuation of the soft robot, we simulate the voltage-induced deformation by the finite element method (Fig. 3C). The results presented in Figure 3C are calculated using ABAQUS 6.12. A material model is embedded into the software with the user-defined subroutine UMAT. Hybrid reduced integration elements (CAX8RH) are used in the simulation.

The robot returns to the rest state when the voltage is not applied, elongates the span of the body when both V_L and V_R are applied, turns right when V_L is applied, and turns left when V_R is applied. When a cyclic voltage is applied, the body deforms cyclically. We achieve locomotion of the robot

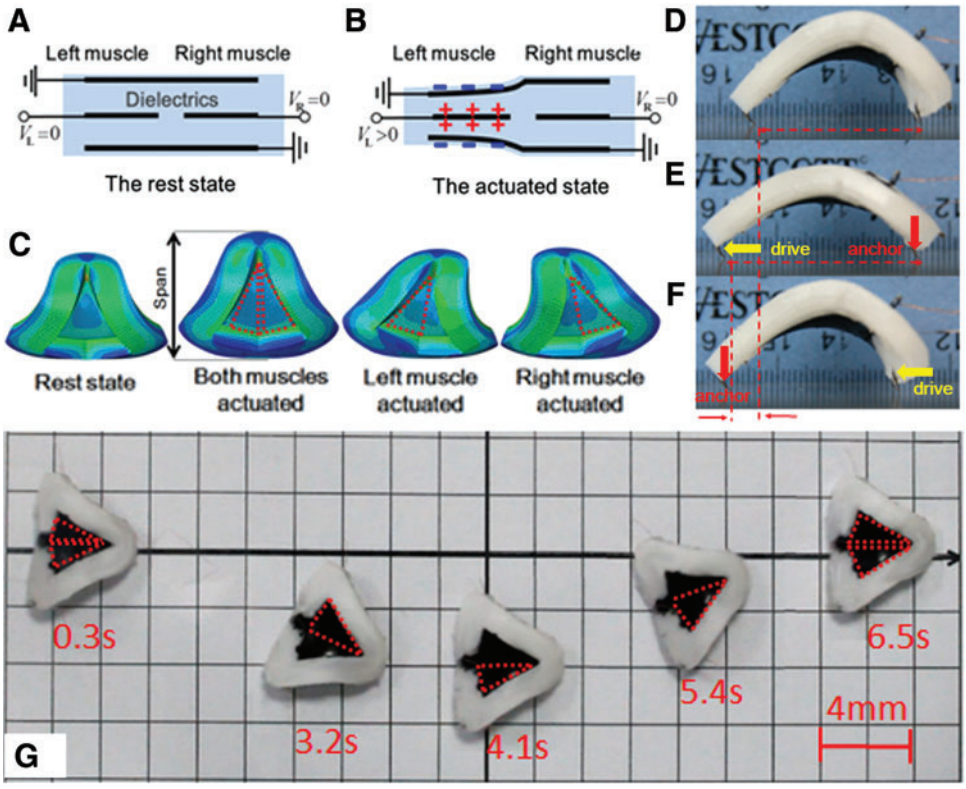

FIG. 3. Actuation and locomotion. **(A)** The cross-sectional view shows that the two feed lines supply separate voltages V_L and V_R to the left and right muscles. When both voltages are turned off, the muscles are in their rest state. **(B)** When V_L is applied, electric charges accumulate on the faces of the dielectrics, causing the left muscle to deform. **(C)** Turn the voltages off to return to the rest state, actuate both muscles to move forward, actuate the left muscle to turn right, and actuate the right muscle to turn left. **(D)** The three hooks point to the backward direction and act as ratchets. In the rest state, the voltage is turned off, and the span—the distance between the front foot and hind feet—is small. **(E)** Upon actuation, the span increases. The front foot moves forward, but the hind feet are anchored. **(F)** When the voltage is turned off, the robot returns to the rest state, the front foot is anchored, but the hind feet move forward. **(G)** The robot runs at a speed of $\sim$100 mm/s, and makes turns. Color images available online at www.liebertpub.com/soro

by applying cyclic voltages to the muscles. In the rest state, the voltage is turned off and the span of the body is small (Fig. 3D). When a voltage is applied, the span increases, the front foot moves forward, but the hind feet are anchored (Fig. 3E). When the voltage is turned off, the span decreases, the front foot is anchored, but the hind feet move forward; the robot returns to the rest state (Fig. 3F). The cyclic applied voltage causes a cyclic deformation of the robot; however, the hooks bias the friction and ratchet the robot forward. Figure 3D–F show the locomotion of the robot in one cycle of the voltage applied as a square wave of frequency 2 Hz and amplitude 8 kV. Because of the biased friction of the feet, when the span of the robot increases, the hind feet anchor and the front foot drives forward. When the span of the robot decreases, the hind feet drive forward and the front foot anchors. The soft robot moves with the alternatively anchoring and driving of the front foot and hind feet. When the actuating frequency is low (1–10 Hz), the soft robot crawls with the discrete moves of the front and hind feet. Thanks to the fast response of the DE actuator, when the actuating frequency rises to 10–40 Hz, the soft robot moves successively, that is, the soft robot runs. We operate the robot to run and turn on a flat silicone pad (Supplementary Movie S1; Supplementary Data are available online at www.liebertpub.com/soro). When the voltages are switched on or off, the robot starts, stops, or turns rapidly. Measured from the top view video, the robot runs forward with both the left and right muscles in actuation (9 kV and 16 Hz), reaching the maximum speed of 161 mm/s, that is, 4 body lengths per second. The high voltage, applied on the right and left muscles of the soft robot, is controlled by an external circuit (Fig. 4). The movements of the robot correspond closely to the sequences of the voltages applied to the left and right muscles (Fig. 5A). We measure the average running speed and turning radius by analyzing the recorded video (Fig. 3G). Within 4 s, the robot runs at an average speed of 110 mm/s (2.75 body lengths per second) and makes three turns with the minimum turning radius of 160 mm (Fig. 6). This DE-driven soft robot runs faster than the other two typical soft robots. A pneumatic-driven soft robot[5] with the body length of 14.2 cm can reach the speed of 0.75 cm/s (0.053 body length per second). A shape memory alloy-driven soft robot[28] with the body length of 30.5 cm can reach the speed of 0.525 cm/s (0.017 body length per second). We have measured the noise of the soft robot during the running (the driven voltage of 10 Hz and 8 kV). A noise meter is fixed above (10 cm) the running track of the soft robot. The measured background noise is 45.1 dB. When the soft robot is running through for 10 times, the measured value varies in the range of 45.1–45.8 dB, indicating the low noise of the soft robot.

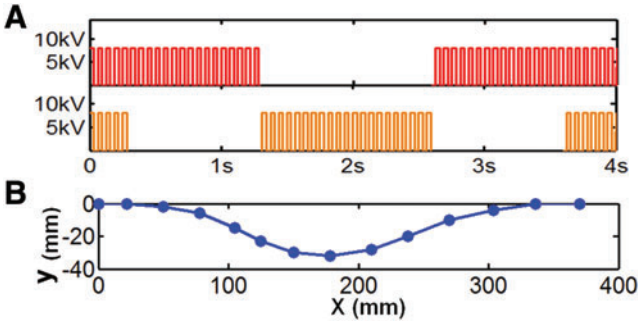

FIG. 5. Measurement of speed and turning. **(A)** The voltage sequence applied on the left and right muscle of the soft robot during the running and turning in Figure 3g. **(B)** The trajectory of the robot. Each *dot* corresponds to the position of the robot (the middle point between two hind feet) from 0 to 3.9 s with the time increment of 0.3 s. Color images available online at www.liebertpub.com/soro

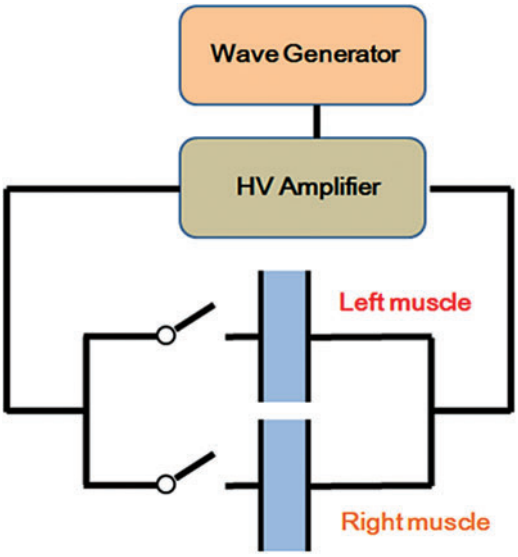

FIG. 4. The power source and external circuit. Schematic representation of the wave generator, HV amplifier, external circuit, and the muscles in the soft robot. HV, high voltage. Color images available online at www.liebertpub.com/soro

Results and Discussion

In this study, we present the modeling and characterization of the soft robot. The soft robot can quickly run and turn without complex fabrication and control, which are difficult to implement with fully soft materials at small scale. The speed of the robot is close to the speeds of legged insects, such as beetles and ants, and is much higher than the speeds of crawling insects, such as caterpillars and inchworms. Despite the challenge for the lifetime of the materials (resulted by the cyclic loading of high voltage), the voltage-driven actuating mechanism of DE provides the advantages of quick response and easy control for the soft robot.

The high speed of our robot is achieved by the mechanism of actuation and locomotion. Indeed, the electrostatic actuation is fast. Although the resistance of the conformal electrodes (carbon grease) is large, $R = 3000\ \Omega$, the capacitance is

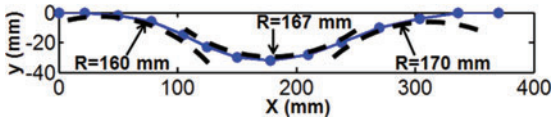

FIG. 6. The average running speed and the turning radius. These can be measured by analyzing the time and the corresponding positions. Color images available online at www.liebertpub.com/soro

small, $C = 64$ pF. The delay time due to charging the actuator is $RC \sim 10^{-7}$s. To further investigate the dynamic behavior of the soft robot, we have measured the structural and mechanical parameters of the soft robot. The effective stiffness of the soft robot in the length direction is measured as follows. The hind feet of the soft robot are fixed on a force sensor, whereas the front foot is free. When the soft robot is stretched along the direction of the span, the reaction force measured from the force sensor equals to the force along the direction of span. A grip pulls the front foot and increase the span of the soft robot; the span of the soft robot and the reaction force of the force sensor are simultaneously recorded by the camera. The relation between the force along the span and the span of the robot is plotted to estimate the effective stiffness of the soft robot along the direction of the span. The robot has an effective mass of $m = 5$ g and effective stiffness of $k = 25$ N/m (Fig. 7A). The period of mechanical resonance can be estimated as $2\pi\sqrt{m/k} \sim 90$ms, and the calculated resonance frequency is around 11 Hz. When robot oscillates freely without touching the ground, the actuation force is about $\varepsilon LV^2/H \sim 0.12$N. The span is $s \sim \varepsilon LV^2/(Hk) = 9.2$mm. This static span is insensitive to the frequency up to mechanical resonance (Fig. 7B). We have also measured the resonance frequency and the vibration amplitude of the soft robot by vibration test. The soft robot is fixed at one end as a cantilever beam. Various voltage signals are applied to the soft robot. High-speed camera recorded the vibration behavior from the side view (Fig. 7B). The measured resonance frequency is about 15 Hz, with the span of 10 mm. Consequently, the response of the robot is not limited by electrical delays but is limited by mechanical resonance. This situation is similar to many designs of electrostatic actuators.[29] We operate the robot by applying voltage near the mechanical resonance, at a frequency of 16 Hz, or a period of 62.5 ms.

The speed of the robot depends on the amplitude and frequency of the applied voltage (Fig. 8A). Multiple tests have been carried out with various voltages and frequencies. The robot reached a constant speed at a voltage and a frequency (e.g., 8 kV and 20 Hz). In each test, we have measured the running distance in 10 s of the robot (recorded by the video camera from top view) to calculate its average speed. The experimental data (empty triangles in Fig. 8A) shows the speed–frequency relation of the soft robot with the voltage amplitude of 7 and 8 kV. The speed of the robot rises as the frequency increases, peaks around a certain frequency, and then decreases. This speed curve indicates that the speed is nearly proportional to the frequency when the frequency is relatively low. When the frequency is around the mechanical resonance, the span is large and the speed of the robot is also large. When the frequency goes beyond the mechanical resonance, the span drops steeply, leading to vanishing speed of the robot. The schematic representation of the dynamic model is shown in Figure 8B. This dynamic model focuses on the forward motion without turning and represents the robot using two degrees of freedom, the displacements of the front and hind feet x_F and x_H of the soft robot. We model the body of the robot by two masses m_F and m_H, and the muscle by a spring connected between the two masses with an effective stiffness k and an excitation force F. The excitation force F in the model corresponds to the voltage actuating the soft DE membrane, releasing and bending the frame with various spans. We assume that the front foot and hind feet will be perfectly anchored on the substrate with no backward slip. Frictional forces f_F and f_H are applied on the feet of the robot as the damping forces. The frictional forces are modeled with the combination of two different friction schemes: viscous friction and Coulomb friction.[28] In viscous friction, the friction force is proportional to the velocity of movement. In Coulomb friction, the friction force is constant. As the soft robot weights 5 g in total, two masses $m_F = 3.5$ g and $m_H = 1.5$ g connected by a spring are used in the model. The stretch of DE membrane in the actuation direction may be modulated, whereas the stretch perpendicular to that direction keeps the same as the prestretch, that is, $\lambda_{2A} = \lambda_{2p} = 2$. During actuation, DE membranes are subjected to the voltage Φ, introducing the Maxwell stress. The body and the muscle of the robot are modeled as a spring with an effective stiffness k.

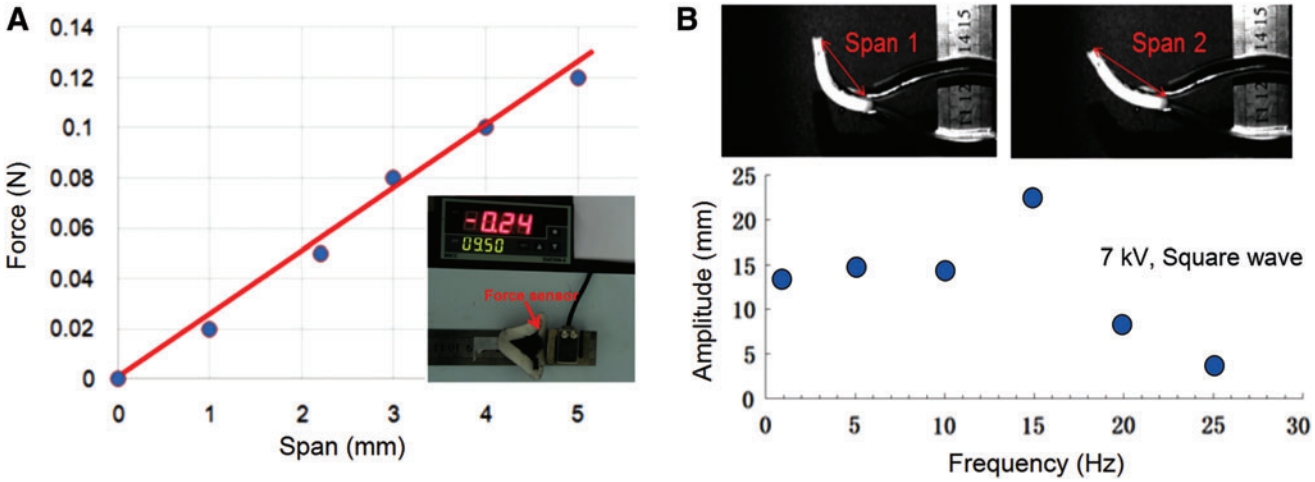

FIG. 7. Measurement of effective stiffness and resonance. **(A)** The force–span relation of the soft robot as a bending beam. The subfigure shows the setup of measurement with the force sensor. **(B)** Before crawling on ground, vibration tests are carried out to find the vibration behavior and the range of operation. The relation of amplitude and frequencies (7 kV, *square wave*) is plotted. Color images available online at www.liebertpub.com/soro

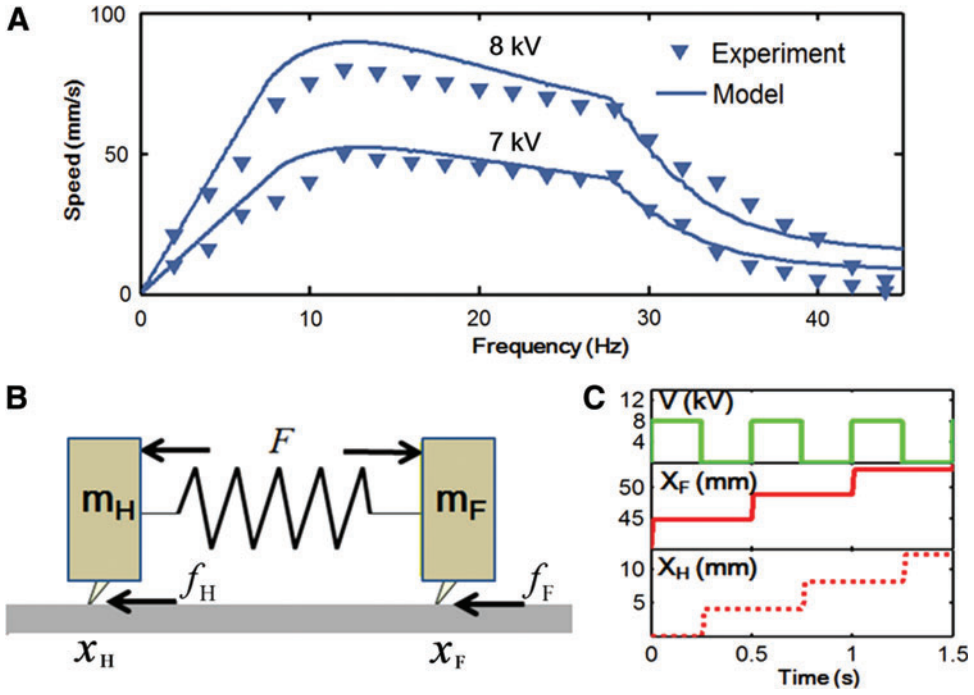

FIG. 8. The model of the ratcheting robot. **(A)** The speed of the robot increases with the amplitude of the applied voltage and maximizes at some intermediate frequency of the applied voltage. The experimental data agree well with the predictions of the model. **(B)** The model characterizes the body of the robot by a spring and two masses and represents the muscles by an actuation force F. Frictional forces f_F and f_H act on the front and hind feet. **(C)** When a square-wave voltage is applied, the biased friction causes the front and hind feet to move and stop alternately. The robot ratchets forward. Color images available online at www.liebertpub.com/soro

The total force (excitation force) applied on the two masses can be expressed as:

$$F = \lambda_{1A}\lambda_{2A}^2 \varepsilon \Phi^2(t) L_w / H, \tag{1}$$

where $\varepsilon = 4\times10^{-12}$F/m is the permittivity, $H = 1$ mm is the initial thickness, and $L_w = 10$ mm is the initial width of the DE membrane (DE membrane with effective area). The length of the robot in the rest state is $a = 40$ mm. λ_{1A} and λ_{2A} are the stretches of the DE membrane in the length and width directions. When the driving force is lower than the maximum static friction, the feet do not move. When the driving force exceeds the maximum static friction, the feet move. We assume that the friction of soft robot belongs to the two regimens of dry friction, the static friction when the robot does not move and the kinetic friction when the robot moves. As there are one front foot and two hind feet, the friction on m_H is $f_H = 2f$ and the friction on m_F is $f_F = f$. The total friction force is $f_F + f_H$, which can be measured from the experiments. The hind of the soft robot is fixed on the force sensor. The soft robot is standing on the surface, while the force sensor is hung above the surface. The force sensor and the soft robot are pushed forward on the surface. The reaction force ~ 0.09 N measured from the force sensor equals to the friction force of the soft robot. The position of the front foot x_F and the hind feet x_H are coupled by the spring connected between the two masses with an effective stiffness k and an excitation force F. The force of the spring and the excitation force F keep being updated during the calculation with current x_F and x_H. As the locomotion mode of the soft robot, the front and hind feet alternatively anchor and drive, the robot can be modeled as a two masses system connected by a spring (Fig. 8B). The soft robot has a triangle-like shape, resulting its hind part about twice the weight of its front part. We model the inertia effect of the robot by separating its total mass (5 g) into the front part (1.5 g) and the hind part (3.5 g).

Starting from the rest state, the driving force pushes the front foot forward ($\frac{dx_F}{dt} > e$, we set $e = 1\times10^{-6}$ m/s), the hind feet are anchored, and the equation of motion for the front foot is

$$m_F \frac{d^2x_F}{dt^2} = -k(x_F - x_H - a) + F - f_F. \tag{2}$$

When the front foot stops ($\frac{dx_F}{dt} \le e$), the driving force pull the hind feet forward, the front foot is anchored, and the equation of motion for the hind feet is

$$m_H \frac{d^2x_H}{dt^2} = -k(x_F - x_H - a) - F - f_H. \tag{3}$$

The equations of motion are solved by MATLAB codes.

The natural frequency of the soft robot can be expressed as $\omega_0 = \sqrt{k/(m_H + m_F)}$, which gives the nondimensional frequency as $\tilde{\omega} = \omega/\omega_0$. The nondimensional speed of the soft robot can be expressed as $\tilde{v} = v\omega_0/a$. Figure 8C shows the movement of m_F and m_H and the voltage (square wave 2 Hz, 8 kV) applied to actuate the robot. The running speeds in various frequencies of soft robot from the analytical model agree well with the experimental results (Fig. 8A). During each operation cycle of the soft robot, the energy input is the electrostatic energy difference of the robot in the rest state and the actuated state. The DE membrane will be charged to reach a high voltage and be short to turn off the voltage. The capacitance of the soft robot in the rest state and the actuated state is around 30–35 pF when the applied voltage is square-wave voltage of amplitude 9 kV and frequency $f = 16$ Hz. The energy input in each operation cycle is 2.8×10^{-3} J. The input power is 44.8 mW. The power density of the robot is around 9 mW/g, which resulted by the large body weight of 4.9 g and the relatively small muscle weight of 0.1 g.

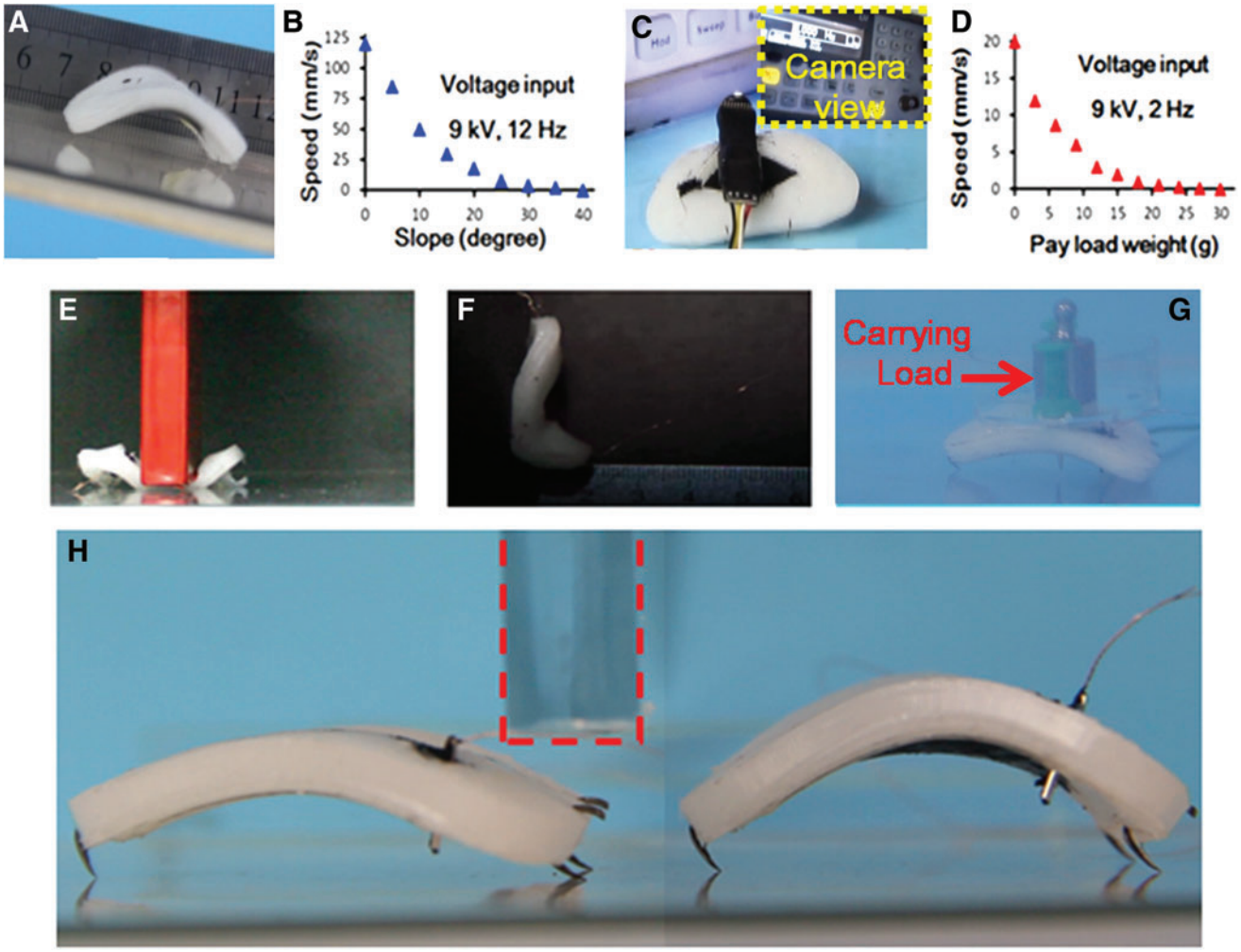

FIG. 9. Robot used and abused. **(A)** The robot climbs on an inclined plane. **(B)** The speed of the robot as a function of the slope of the inclined plane. **(C)** The robot carries a payload (a camera). The *inset* shows the view from the camera. **(D)** The speed of the robot as a function of the weight of the payload. The robot itself weighs 5 g. **(E)** A heavy load flattens the robot. When the load is removed, the robot recovers its shape and runs again. **(F)** The robot hits the rigid wall at the speed around 30 m/s and bounces back. After the impact, the robot remains functional. **(G)** The robot is water proof and can run in hot water. **(H)** The robot sneaks through a narrow seam half its height (the *red dashed lines* indicates the upper boundary of the narrow seam). Color images available online at www.liebertpub.com/soro

Applications of soft robots, such as in field exploration, require the soft robot to overcome complex terrains, carry payload, and survive tough environments.[30,31] The soft robot can climb slope and carry camera as the functional payload (Supplementary Movie S1). The robot can climb on an inclined plane made of an acrylic polymer covered with a silicone pad (Fig. 9A). The climbing speed decreases as the slope increases and vanishes when the slope reaches 30° (Fig. 9B). The robot can carry a payload many times of its own weight, such as a video camera (Fig. 9C). The robot itself weighs 5 g. The running speed decreases as the payload increases and vanishes when the payload reaches 30 g (Fig. 9D). To demonstrate the resilience of the soft robot, we perform the compression test on the robot during its running. The robot is running at a speed of around 30 mm/s (square-wave voltages with the amplitude of 8 kV and the frequency of 20 Hz). A flat punch firmly compresses on the robot during its operation (Fig. 9E; Supplementary Movie S2). The compressive force and the deformed configuration are monitored simultaneously. During the test, the voltage keeps unchanged, actuating the robot. When the punch releases, the robot recovers its operation status and runs again. The robot survives the compressive force up to 1.55 kN during the operation without mechanical fracture or electrical breakdown. Accounting for the cross-section of the indenter (1×5 cm), the pressure (3.1 MPa) is twice that induced by human steps (a human weighs 60 kg and with two feet contact area of $17 \times 10 \times 2$ cm). This compression test proves that mechanical abuse with the same level of human steps cannot destroy the robot. The robot can also survive high-speed impact to the rigid substrate (Fig. 9F; Supplementary Movie S3). The robot is highly elastic, absorbing the energy of impact and bouncing back. The impact speed can reach 30 m/s without breaking the soft robot. This speed is comparable to the terminal speed of the robot during free-falling (with the sectional area of 20 cm^2 and weight of 5 g). The robot can

survive the falling from arbitrary height, which is a great advantage for distributing the robot from air without parachute or protection cover. The high voltage of the soft robot can be insulating cover, and the robot can operate under water, run or swim (Fig. 9G; Supplementary Movie S4). The soft robot can operate under the hot and cold water in a wide temperature range from 0.5 to 90°C, in which the soft robot based on shape memory alloy or polymer may difficult to operate. As the material and the structure of the soft robot are incompressible, the soft robot can operate in the vacuum or under high hydraulic pressure, whereas the pneumatic soft robot may be difficult to operate. The wide range of operation gives the soft robot good resilience in tough environments. A unique advantage of the soft robot is that the soft robot can squish itself to pass through a narrow seam. Figure 9H shows that the soft robot passing through a narrow seam (highlighted by red dashed line), which is half of the robot's height. The robot will stack by the seam with regular operating methods. A DC voltage is first applied on the robot to further bend the robot with lower than the seam, then the AC voltage is applied to induce the locomotion. The robot successfully passes through the seam.

The DE membranes in the soft robot require high voltage for actuation. The compact powering system includes the lithium ion battery and the high voltage boosting electronics. In the future design of the soft robot, compact system with high voltage power and control[11] may be installed on board. For the design and fabrication of the untethered running soft robot, the grand challenge remains in the compact and light weight of the powering and control system and the driving force of the soft artificial muscle. Lowering the actuating voltage of the soft material with new materials (e.g., flexible piezo and ferroelectric materials) and structures (multiple stacks of thin DE films to lower actuating voltage) may enhance the performance of the soft robot in future studies.

Conclusions

In summary, we have developed a DE actuated soft robot to achieve fast motion, high resilience, and low noise. The soft DE robot provides a platform to stimulate the development of many technologies, such as stretchable capacitor, battery, voltage amplifier (for autonomy), and stretchable transistor (for communication and wireless control). Recently developed transparent electrodes and compact voltage amplifiers may soon enable autonomous and all transparent soft DE robot.

Acknowledgments

This work is supported by the National Natural Science Foundation of China (Grant Nos. 11525210, 11621062, 91748209, 11432012, 11572280, and U1613202), the Zhejiang Provincial Natural Science Foundation of China (Grant Nos. LZ14A020001 and LR18A020001), the China Association for Science and Technology (Young Elite Scientist Sponsorship Program No. YESS20150004), the Fundamental Research Funds for the Central Universities, and NSF MRSEC (Grant No. DMR-1420570). Patent applications ''Soft dielectric elastomer robot'' and ''Soft dielectric elastomer robotic actuators'' have been filed but not yet published.

Data and Materials Availability

Contact S.Q. and Z.S. for materials and data requests.

Author Disclosure Statement

No competing financial interests exist.

References

1. Resh VH, Cardé RT, Resh VH, et al. *Encyclopedia of Insects*. Amsterdam: Elsevier/Academic Press, 2009.
2. Hoffman KL, Wood RJ. Myriapod-like ambulation of a segmented microrobot. Auton Robot 2011;31:103–114.
3. Sanchez CJ, Chiu CW, Zhou Y, et al. Locomotion control of hybrid cockroach robots. J R Soc Interface 2015;12: 1–9.
4. Trimmer MB, Ewoldt PRH, Kovac M, et al. At the crossroads: Interdisciplinary paths to soft robots. Soft Robot 2014;1:63–69.
5. Shepherd RF, Ilievski F, Choi W, et al. Multigait soft robot. Proc Natl Acad Sci USA 2011;108:20400.
6. Morin SA, Shepherd RF, Kwok SW, et al. Camouflage and display for soft machines. Science 2012;337:828–832.
7. Breedon P, Coulter F, Vloeberghs M. Dynamic facial prosthetics for sufferers of facial paralysis. Med J Australia 2011;4:555–562.
8. Brown E, Rodenberg N, Amend J, et al. Universal robotic gripper based on the jamming of granular material. Proc Natl Acad Sci USA 2010;107:18809–18814.
9. Trimmer BA. A journal of soft robotics: Why now? Soft Robot 2013;1:1–4.
10. Tian B, Liu J, Dvir T, et al. Macroporous nanowire nanoelectronic scaffolds for synthetic tissues. Nat Mater 2012;11:986–994.
11. Li T, Li G, Liang Y, et al. Fast-moving soft electronic fish. Sci Adv 2017;3:e1602045.
12. Polygerinos P, Wang Z, Galloway KC, et al. Soft robotic glove for combined assistance and at-home rehabilitation. Robot Auton Syst 2014;73:135–143.
13. Tolley MT, Shepherd RF, Mosadegh B, et al. A resilient, untethered soft robot. Soft Robot 2014;1:213–223.
14. Su Z, Yu J, Tan M, et al. Implementing flexible and fast turning maneuvers of a multijoint robotic fish. IEEE ASME Trans Mechatron 2014;19:329–338.
15. Lu N, Kim DH. Flexible and stretchable electronics paving the way for soft robotics. Soft Robot 2014;1:53–62.
16. Martinez RV, Branch JL, Fish CR, et al. Robotic tentacles with three-dimensional mobility based on flexible elastomers. Adv Mater 2013;25:205–212.
17. Lin HT, Leisk GG, Trimmer B. GoQBot: a caterpillar-inspired soft-bodied rolling robot. Bioinspir Biomim 2011; 6:026007.
18. Ma KY, Chirarattananon P, Fuller SB, et al. Controlled flight of a biologically inspired, insect-scale robot. Science 2013;340:603.
19. Calisti M, Giorelli M, Levy G, et al. An octopus-bioinspired solution to movement and manipulation for soft robots. Bioinspir Biomim 2011;6:036002.
20. Lipson H. Challenges and opportunities for design, simulation, and fabrication of soft robots. Soft Robot 2013;1: 21–27.
21. Chan V, Park K, Collens MB, et al. Development of miniaturized walking biological machines. Sci Rep 2012;2:857.
22. Ewoldt RH. Extremely soft: Design with rheologically complex fluids. Soft Robot 2014;1:12–20.

23. Hu DL, Bush JWM. Meniscus-climbing insects. Nature 2005;437:733.
24. Anderson IA, Gisby TA, Mckay TG, et al. Multi-functional dielectric elastomer artificial muscles for soft and smart machines. J Appl Phys 2012;112:041101–041120.
25. Li T, Keplinger C, Baumgartner R, et al. Giant voltage-induced deformation in dielectric elastomers near the verge of snap-through instability. J Mech Phys Solids 2013;61: 611–628.
26. Carpi F, Bauer S, De Rossi D. Stretching dielectric elastomer performance. Science 2010;330:1759–1761.
27. Anderson IA, Hale T, Gisby T, et al. A thin membrane artificial muscle rotary motor. Appl Phys A 2010;98:75–83.
28. Seok S, Onal CD, Cho KJ, et al. Meshworm: A peristaltic soft robot with antagonistic nickel titanium coil actuators. IEEE ASME Trans Mechatron 2013;18:1485–1497.
29. Keplinger C, Sun J-Y, Foo CC, et al. Stretchable, transparent, ionic conductors. Science 2013;341:984–987.
30. Brochu P, Pei Q. Advances in dielectric elastomers for actuators and artificial muscles. Macromol Rapid Commun 2010;31:10–36.
31. Full RJ, Tu MS. Mechanics of a rapid running insect: Two-, four- and six-legged locomotion. J Exp Biol 1991;156:215.

Address correspondence to:
Shaoxing Qu
Department of Engineering Mechanics
Zhejiang University
38 Zheda Rd.
Hangzhou 310027
China

E-mail: squ@zju.edu.cn

Zhigang Suo
John A. Paulson School of Engineering and Applied Sciences
Kavli Institute for Nanobio Science and Technology
Harvard University
29 Oxford St.
Cambridge, MA 02138

E-mail: suo@seas.harvard.edu